Respiratory activity in the facial nucleus in an *in vitro* brainstem of tadpole, *Rana catesbeiana*

G.-S. Liao*, L. Kubin*†‡, R. J. Galante*, A. P. Fishman*†§ and A. I. Pack*†‖

*Centre for Sleep and Respiratory Neurobiology, †Pulmonary and Critical Care Division, Department of Medicine, and ‡Department of Animal Biology, School of Veterinary Medicine and §Department of Rehabilitation Medicine, University of Pennsylvania, Philadelphia, PA, USA

1. In studies of the central neural control of breathing, little advantage has been taken of comparative approaches. We have developed an *in vitro* brainstem preparation using larval *Rana catesbeiana* which generates two rhythmic neural activities characteristic of lung and gill ventilation. Based on the pattern of the facial (VII) nerve activity both lung and gill rhythm-related respiratory cycles were divided into three distinct phases. The purpose of this study was to characterize and classify membrane potential trajectories of respiratory motoneurons in the VII nucleus at intermediate stages (XII–XVII) of development.

2. Seventy five respiratory-modulated neurons were recorded intracellularly within the facial motor nucleus region. Their resting membrane potential was between −40 and −80 mV. Sixty of them were identified as VII motoneurons and fifteen were non-antidromically activated. Membrane potentials of fifty-six of the seventy-five neurons were modulated with both lung (5–27 mV) and gill rhythms (3–15 mV) and the remaining nineteen neurons had only a modulation with lung rhythmicity (6–23 mV). No cells with gill modulation alone were observed.

3. All of the cells modulated with lung rhythmicity had only phase-bound depolarizing or hyperpolarizing membrane potential swings which could be categorized into four distinct patterns. In contrast, of the fifty-six cells modulated with gill rhythmicity, thirty-two were phasically depolarized during distinct phases of the gill cycle (four patterns were distinguished), whereas the remaining twenty-four were phase spanning with two distinct patterns. The magnitudes of lung and gill modulations were proportionally related to each other in the cells modulated with both rhythms.

4. In all sixteen neurons studied, a reduction or a reversal of phasic inhibitory inputs during a portion of the lung or gill respiratory cycle was observed following a negative current or chloride ion (Cl^-) injection. The phasic membrane resistance modulation in relation to the gill rhythm was analysed in six neurons and a relative decrease in the somatic membrane resistance (0·7–8·1 MΩ) was detected during the periods of hyperpolarization.

5. We propose that, at these intermediate stages of development: (a) both gill and lung respiratory oscillations in motoneurons are generated by respiratory premotor neurons having only a few distinct activity patterns; (b) these patterns delineate distinct portions of the centrally generated respiratory cycles; and (c) phasic synaptic inhibition, mediated by Cl^-, contributes to shaping the membrane potential trajectories of respiratory motoneurons.

Most of the information about respiratory rhythmogenesis and homeostatic mechanisms controlling the respiratory output has been obtained from studies in mammals. Respiratory neurons have been studied extensively using extra- and intracellular recordings, and neuroanatomical techniques. The studies have been performed mostly in cats,

‖ To whom correspondence should be addressed at the Centre for Sleep and Respiratory Neurobiology, Hospital of the University of Pennsylvania, Philadelphia, PA, USA.

rabbits or rats (see Ezure, 1990, for references) and, more recently, in the neonatal rat preparation of an isolated brainstem and spinal cord *in vitro* (Suzue, 1984; Feldman & Smith, 1989; see Berger, 1990; Feldman *et al.* 1990 for reviews). A major goal of many of these studies has been to explain the neural processes of generating respiratory rhythm and to elucidate the neural mechanisms that shape the pattern of the respiratory motor output.

In the studies of respiratory rhythmogenesis, relatively little advantage has been taken of comparative approaches. Although the mechanical aspects of breathing and gas exchange have been extensively studied in many species representative of various evolutionary stages (deJongh & Gans, 1969; West & Jones, 1975; Burggren & West, 1982; West & Burggren, 1982, 1983; Shelton, Jones & Milsom, 1986), the corresponding knowledge of the central neural mechanisms of respiratory control is very limited. This is in contrast to extensive studies of other rhythmic behaviours such as stepping or swimming (e.g. Russell & Wallén, 1983; Cohen, Dobrov, Li, Kiemel & Baker, 1990; Sillar, Wedderburn & Simmers, 1991; Sillar, Simmers & Wedderburn, 1992) which have demonstrated that a comparative approach can be helpful in gaining new insights into the underlying neural circuits in mammals.

One species in whom gas exchange and mechanical events associated with breathing have been rather extensively studied are amphibians. They represent an interesting case of lower vertebrates in which phylogenetically older forms of gas exchange through skin and gills coexist with positive pressure lung ventilation. Both larval and adult forms of amphibians have well developed lung and airway mechanoreceptors and chemoreceptors that can modulate breathing in a manner similar to that in mammals (see Shelton *et al.* 1986, for references). Moreover, in their development from larvae to adult, amphibians such as bullfrogs undergo a transformation from aquatic breathers using their gills to air breathers using pulmonary gas exchange (Burggren & West, 1982; Burggren, 1984; Burggren & Just, 1992). Consequently, study of the central neural mechanisms of respiratory rhythmogenesis and regulation in amphibians offers a unique opportunity to gain new insights into the origin, maturation and properties of a respiratory rhythm generator.

The *in vitro* brainstem preparation in larval *Rana catesbeiana* (Galante, Smith, Kubin & Pack, 1992; Pack, Galante, Walker, Kubin & Fishman, 1993) provides a good model for such studies. Tadpoles of *Rana catesbeiana* change their respiratory function from aquatic to air breathing during their metamorphosis. Their morphological development has been described in great detail, with twenty-five distinct developmental stages (Taylor & Kollros, 1946). Initial studies from our laboratory (Galante *et al.* 1992; Pack *et al.* 1993) have established that the neural respiratory activity in an isolated tadpole brainstem corresponds closely to the patterns observed in intact amphibian larvae (West & Burggren, 1982, 1983). The respiratory motor output at intermediate stages of development shows two characteristic rhythmicities, one corresponding to gill ventilation and the other to lung ventilation.

The aim of the present study was to investigate the patterns of respiratory activities related to lung and gill ventilation in individual motoneurons, using isolated brainstems of tadpoles at developmental stages XII–XVII, i.e. when both gill and lung respiratory rhythmicities are present. Study of the respiratory synaptic inputs that impinge on motoneurons provides an insight into the patterns of activities in premotor respiratory neurons. Therefore, this study is an important first step in subsequent study of the developmental changes in the circuits that generate the respiratory motor output in amphibians. We recorded intracellularly from facial (VII) motoneurons and other respiratory cells within the VII nucleus since the VII nerve innervates major respiratory muscles in this species (deJongh & Gans, 1969; see Nieuwenhuys & Opdam, 1976, for references). We utilized intracellular recording since our goal was also to assess the presence and pattern of the convergence of the phasic lung and gill-related inputs that, as our results show, are both excitatory and inhibitory.

Preliminary results of this study have been published in an abstract form (Liao, Kubin, Galante, Pack & Fishman, 1993).

METHODS

Preparation of the *in vitro* brainstem

Experiments were performed on forty tadpoles (*Rana catesbeiana*). Specimens at developmental stages XII–XVII (Taylor & Kollros, 1946) were selected because they use both gills and lungs for ventilation (Burggren & West, 1982). Before the experiments, commercially supplied tadpoles (Nasco, Fort Atkinson, WI, USA) were housed in aerated and dechlorinated water at 20 ± 2 °C for at least 5 days and fed Purina Trout Chow (Ralston purina Co., St Louis, MO, USA) *ad libitum*.

Tadpoles were anaesthetized by immersion for 10 min in a mixture of tricaine methanesulphonate (MS-222) and dechlorinated water (1 : 10 000) buffered to pH 7·0 with NaOH. They were then placed in a dissecting dish and bathed in oxygenated physiological solution (for composition see below) for the duration of the surgery. A mid-line incision was made on the dorsal surface starting at the body–tail junction and proceeding rostrally above the cranium to the level of the eyes. The muscle and cartilaginous skull was trimmed to expose the brain. The choroid plexus was removed and the floor of the fourth ventricle exposed. The brain was transected first through the mid-diencephalon and then at the spino-medullary junction with bleeding controlled by flushing the area with physiological solution. The cranial nerves were dissected bilaterally and the isolated brainstem was lifted from the skull and transferred to a recording chamber. Surgery was completed in 8–10 min. Subsequently the brainstem was fixed to a layer of Sylgard coating the bottom of the chamber with the dorsal surface up using two stainless-steel pins inserted into non-critical

portions of the tissue. The chamber was perfused with oxygenated physiological solution for a 30–60 min recovery period before starting the recordings.

The recording chamber that we used is similar in design to that used by Smith & Feldman (1987). Solutions were delivered to the brainstem using a gravity perfusion system. The composition of the perfusate used was (mM): NaCl, 78·8; KCl, 3·1; $CaCl_2$, 2·4; $MgSO_4$, 1·2; NaH_2PO_4, 1·2; $NaHCO_3$, 30; and glucose, 3·9. All chemicals were of analytical grade and were dissolved in deionized water. The pH of the medium was maintained at 7·6 ± 0·2 by adjusting the relative proportions of CO_2 (3–5%) and O_2 (95–97%). The appropriate mixture was bubbled through the solution contained in a 500–1000 ml separatory funnel fitted with a jacketed Graham condenser for at least 15–20 min before starting the perfusion and throughout the duration of the experiment. The solution flowed gravitationally through a flow metering valve (Nupro L-series, Nupro Co., Willoughby, OH, USA) and an insulated glass tube into the water-jacketed recording chamber. The outflow port of the recording chamber was connected to a second metering value (Nupro L-series) and a suction line. Both the jacketed recording chamber and the Graham condenser were connected in series with a constant temperature bath circulator (PK2, Haake, Berlin, Germany) which was used to maintain temperature at 20 ± 0·5 °C. The chamber volume was 2·5 ml and the perfusion rate was set at 5–6 ml min^{-1}. The actual temperature and pH of the medium were continuously monitored using a microthermistor probe (Bat 10, Bailey Instrument Co., Saddle Brooke, NJ, USA) and a semi-micro pH probe (91-03, Orion Research Inc., Boston, MA, USA), respectively, both placed in the recording chamber.

Recording and stimulation procedures

Figure 1*A* shows the tadpole brainstem preparation and the arrangement of the recording and stimulating electrodes. Facial nerve activity was recorded using a monopolar suction electrode. The activity was amplified (BMA-830, CWE Inc., Ardmore, PA, USA), filtered (200–2000 Hz), and fed to a moving average circuit

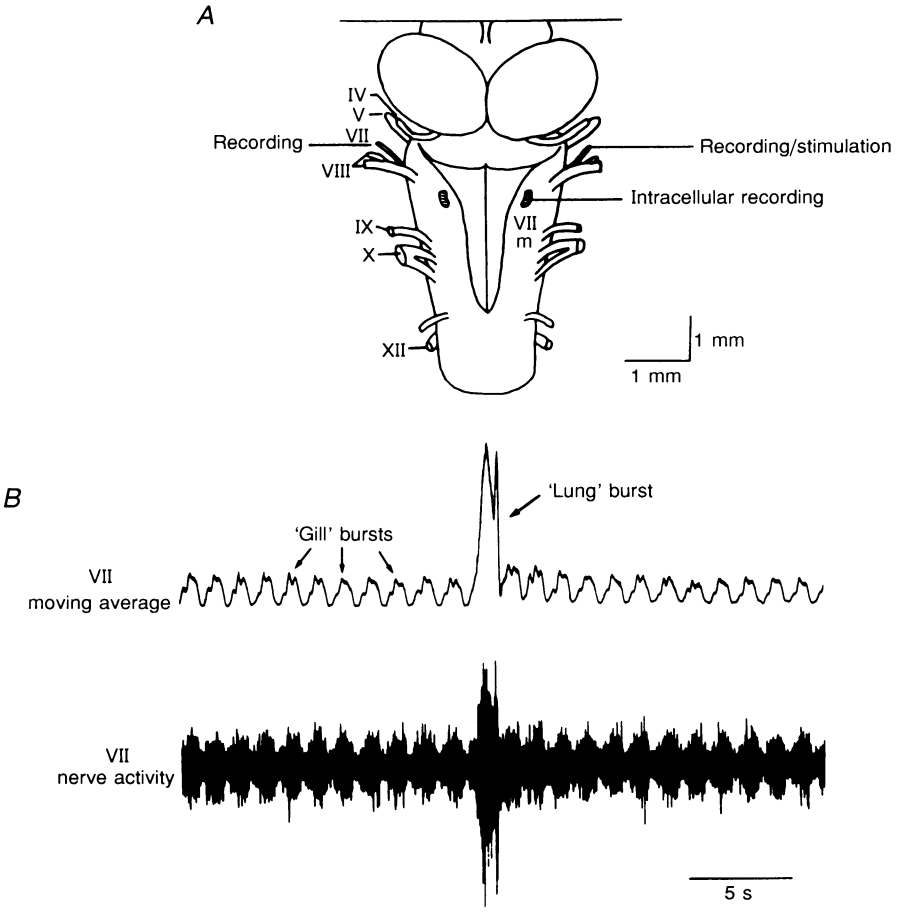

Figure 1. Diagram of the tadpole brainstem *in vitro* (*A*) and an example of the recording of respiratory neural activity from the facial (VII) nerve (*B*)

A, dorsal view of the brainstem of the tadpole illustrating the arrangement of the recording and stimulation electrodes used in this study. IV–XII label the corresponding cranial nerves; VIIm defines the location of the facial motor nucleus. *B*, typical activity recorded from the VII nerve of a tadpole brainstem *in vitro* (developmental stage XV). Two types of rhythmic activities can be identified: one, with a low magnitude and a high frequency, representing fictive gill ventilation; and another, with a high amplitude and a low frequency, representing fictive lung ventilation. Top trace: moving average of the whole VII nerve activity; bottom trace: raw VII nerve activity.

(MA 821, CWE) having a time constant of 100 ms. Initially, the activities of both left and right VII nerves were recorded to verify that both sides displayed a respiratory activity. Subsequently, one of those electrodes was used for antidromic activation of VII motoneurons while the other was for monitoring the respiratory activity.

For antidromic stimulation, current pulses of 0·05–0·1 ms duration having a sufficient intensity (1–25 μA, constant current stimulator; PSIU6, Grass Instruments) were used to evoke an antidromic field potential in the VII nucleus with pulses being applied between the suction electrode and a reference electrode placed in the bath. The evoked field potential was monitored using the AC output of the DC amplifier (see below) and its antidromic character was confirmed using standard criteria of fixed latency and ability to follow one to three stimuli presented at 2–3 ms intervals. For individual neurons, to confirm the antidromic character of the response, a collision test was performed by application of a brief intracellular pulse (0·1 ms) that produced an action potential followed, with various delays, by the stimulus applied to the nerve, and subsequent verification that the studied cells could follow two to three stimuli applied to the nerve at about 300 Hz.

For intracellular recording, glass microelectrodes were pulled using borosilicate (1·2/0·6 mm) or alumino-silicate (1·0/0·58 mm) glass capillary tubing (P-87 puller, Sutter Instrument Co.). The microelectrodes were filled with 2 M potassium acetate or, in the experiments with intracellular chloride ion (Cl^-) injection, with 3 M KCl (DC resistance 30–80 MΩ and about 20 MΩ, respectively). The microelectrode was positioned in the VII motor nucleus area using a stepping motor-controlled manipulator (Nano-Stepper, SPI Wiss, Oppenheim, Germany). Facial motoneurons were searched for near the VII nerve entry level, about 2·6 mm rostral to obex, by moving the microelectrode from mid-line to about 0·4 mm lateral and 50–400 μm below the dorsal surface of the brainstem while applying single stimuli to the VII nerve (1 Hz). Penetrations were usually achieved by causing a brief over-compensation of the capacitance compensation circuit of the amplifier. The intracellular signal was amplified ten times in a DC mode (8700 Cell Explorer, Dagan Corp., Minneapolis, MN, USA) and, for observation of synaptic noise, another ten times in an AC mode (bandwidth 10–2000 Hz; BMA 830 amplifier, CWE). Both the intracellular signal and the VII nerve activity were monitored on an oscilloscope and a chart recorder (ES1000, Gould Instruments) and stored on a magnetic tape (3960 tape recorder, Hewlett-Packard) for subsequent off-line analysis.

For reversing of postsynaptic inhibition, presumably mediated by Cl^-, cells were hyperpolarized up to −90 mV by application of a negative DC current (0·5–2·0 nA). In selected cells recorded with KCl-filled electrodes, Cl^- was injected intracellularly (1–10 nA for 1–8 min).

Assessment of the changes in membrane resistance with gill rhythmicity was performed off-line using an IBM computer-based data acquisition and analysis software (EGAA data analysis package, RC-Electronics Inc., Santa Barbara, CA, USA). Voltage responses to a negative intracellular current pulse (0·5 nA, 50 ms, applied every 1–2 s) were recorded over a period covering twenty to fifty gill cycles. Subsequently, voltage responses occurring in the middle of the maximally depolarized and maximally hyperpolarized portions of the gill cycle were digitized (sampling rate, 10 kHz), measured sequentially, and differences between adjacent responses produced in the opposite phases of the gill rhythm were calculated. An average difference from twenty to fifty such pairs was divided by the magnitude of the current pulse to obtain the difference in the somatic membrane resistance between the two compared phases of the gill cycle.

All recordings of individual motoneurons were begun at least half an hour after placement of the brainstem in the recording chamber and we continued to search for motoneurons for about 6–8 h. Rhythmic neural activities were stable during this period, as assessed by comparing the mass activity recorded from the VII nerve at the beginning and at the end of the session. Determinations of the intracellular membrane potential were based on the voltage increase recorded at the end of recording when the electrode was withdrawn from the cell. Only stable recordings from respiratory-modulated neurons that showed a membrane potential of at least −40 mV during the period of maximal phasic hyperpolarization and a magnitude of the respiratory modulation of at least 3 mV were accepted for further analysis.

Analysis of the patterns of membrane potential trajectories

Based on the characteristic shape of the whole VII nerve activity and its moving average, distinct phases of both gill and lung respiratory cycles were distinguished, as described in the first section of the Results. Determinations of the average durations of the lung and gill cycles and their components were based on the segments of at least 20 min of stable recordings. Individual neurons were initially classified as phase bound when distinct swings in their membrane potential trajectories occurred in synchrony with the phase transition points identified in the whole nerve activity (± 50 ms), or phase spanning when changes in their potential spanned gradually through such transition points. Neurons were classified further with respect to the corresponding phase of the whole VII nerve activity based on the temporal occurrence of the depolarizing swing of the membrane potential in the cell. In a few cells, a clear phasic hyperpolarization rather than a depolarization related to lung rhythmicity could only be identified with certainty. Consequently, these cells were separately classified based on the phase of their hyper- rather than depolarizing input. Cells in which the presence of action potentials could interfere with the assessment of their membrane potential trajectories were actively depolarized by current injection to inactivate the spike-generating mechanisms. Depolarizations rather than hyperpolarizations were used in order to increase any distinct phasic membrane potential swings that might have resulted from postsynaptic inhibition. Those, if present, were studied further by graded applications of DC current of both polarities or Cl^- injections.

All variables in this report are characterized by their means and standard deviations (S.D.), and a paired or unpaired Student's t test was used for evaluation of statistical significance of differences between the means.

RESULTS

Motor output patterns in the facial nerve *in vitro*

In order to classify different activity patterns and membrane potential trajectories in individual neurons, we first evaluated the patterns of the respiratory motor output in the whole VII nerve in sixteen preparations. As reported previously (Galante *et al.* 1992; Pack *et al.* 1993), two types of rhythmic activities are present in the VII nerves

(Fig. 1*B*). One, with low amplitude and higher frequency, corresponds to fictive gill ventilation (buccal oscillations). The other has high amplitude bursts occurring with a much lower frequency and corresponds to fictive lung ventilation. The patterns of these two neural activities correspond to the respiratory mechanical events recorded from peripheral respiratory organs in larvae of *Rana catesbeiana* (West & Burggren, 1983) and have been shown to directly correlate with the simultaneously recorded opercular and lung pressures in tadpoles (Pack *et al.* 1993).

Figure 2*A* shows, on an expanded time scale, an example of typical gill bursts. A more detailed inspection of the neural activity related to gill ventilation reveals that the more active phase consists of two distinct components: a gradually increasing initial component having a relatively low amplitude and short duration, and a second, fast-rising and then slowly decaying component of relatively high amplitude and relatively long duration. Thus, based on these features of the gill-related fictive motor output, we have divided the gill cycle into three phases: G_1 and G_2,

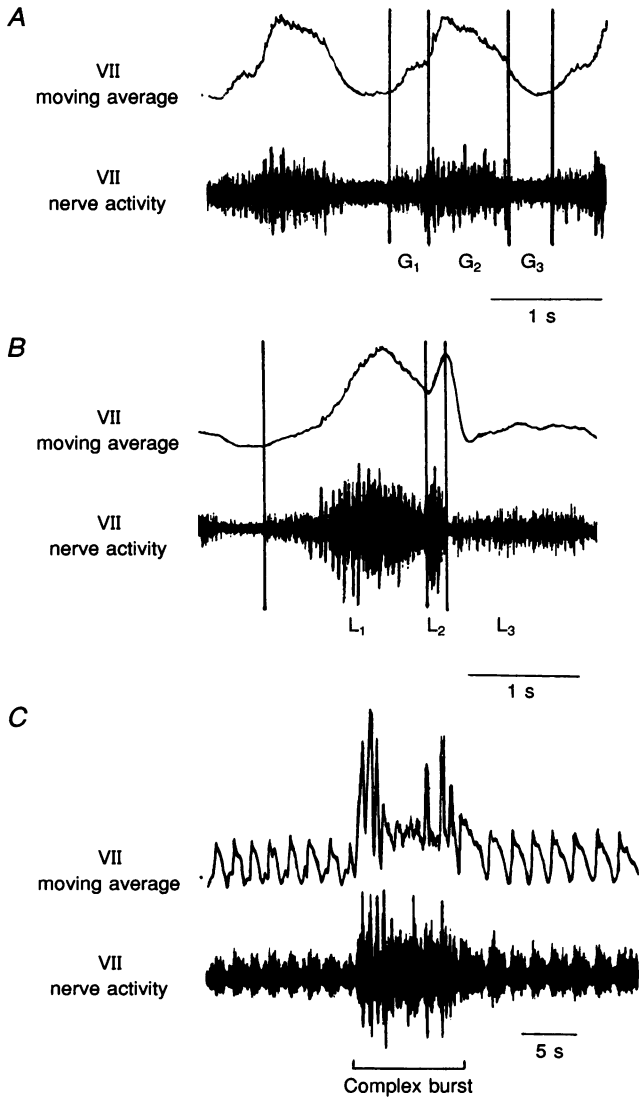

Figure 2. Identification of distinct phases within the gill cycle (*A*) and the lung burst (*B*), based on recording from the facial (VII) nerve

The moving average (top trace) and raw nerve activity (bottom trace) are shown in each panel. *A*, example of a typical gill cycle. Three distinct phases can be distinguished: G_1, corresponding to the first portion of the gill burst; G_2, corresponding to the second portion of the gill burst; and G_3, corresponding to the interval between the bursts. *B*, example of a typical lung burst. Two phases of the burst can be distinguished: L_1, corresponding to the initial, slowly rising phase; and L_2, corresponding to the later, rapidly rising portion of the burst. Phase L_3 corresponds to the period between successive lung bursts. *C*, example of a complex lung burst-like activity. Such bursts often begin with a typical, simple lung burst (as in *B*) followed by a series of irregular bursts lasting 5–25 s. The time scale of this record is different from that in *A* and *B*.

successively occurring during the active portion of the cycle, and G_3, corresponding to the interval between gill bursts. The average duration of the gill cycle across all animals ($n = 16$) was $1{\cdot}4 \pm 0{\cdot}3$ s with the corresponding average durations of the successive phases being $0{\cdot}4 \pm 0{\cdot}1$, $0{\cdot}7 \pm 0{\cdot}1$ and $0{\cdot}3 \pm 0{\cdot}1$ s, for G_1, G_2 and G_3, respectively.

Figure 2*B* shows a typical example of the lung ventilation-related neural burst. This activity also shows at least three distinct phases. The first phase of the lung burst (L_1) has a gradually increasing amplitude and a relatively long duration ($1{\cdot}1 \pm 0{\cdot}3$ s). In most tadpoles, the activity in this phase appeared to increase in two distinct steps, first slowly and then more rapidly, as in Fig. 2*B*. Since we did not find any neurons having activity patterns directly related to either of these sub-phases alone (see below), we decided to treat the activity during phase L_1 as one entity. The activity during the second phase of the lung burst (L_2) is characterized by a sharp peak with a large amplitude and a very short duration ($0{\cdot}2 \pm 0{\cdot}1$ s). The amplitude of the L_1 component of the burst has in the order of 70–100% of the amplitude of the L_2 component. The L_2 component occupies about 15% of the total lung burst duration. The interval between the lung bursts (phase L_3) is occupied by the activity related to the gill rhythm, as described above. This interval is variable, with a mean duration of $1{\cdot}0 \pm 0{\cdot}5$ min as averaged across all animals. In some preparations, a transient suppression of the gill-related activity occurred just before or just after a lung burst, similar to that seen in intact tadpoles (West & Burggren, 1983).

Occasionally, we observed more complex bursts that were of much longer duration than the typical simple lung burst described above (see example in Fig. 2*C*). These bursts were also more variable in their pattern and duration than the latter. About 50% of these complex bursts began with what appeared to be a typical lung burst that was then followed by a number of relatively irregular bursts, so that the total duration of such a 'bout' could be as long as 10–25 s. These complex events occurred once every five to sixty regular lung cycles without any obvious rhythmicity. In some preparations they occurred more frequently than in others without any relationship to the stage of development. They may correspond to what has been termed the lung inflation cycle (deJongh & Gans, 1969). Due to their infrequent occurrence, intracellular data related to these events were not analysed.

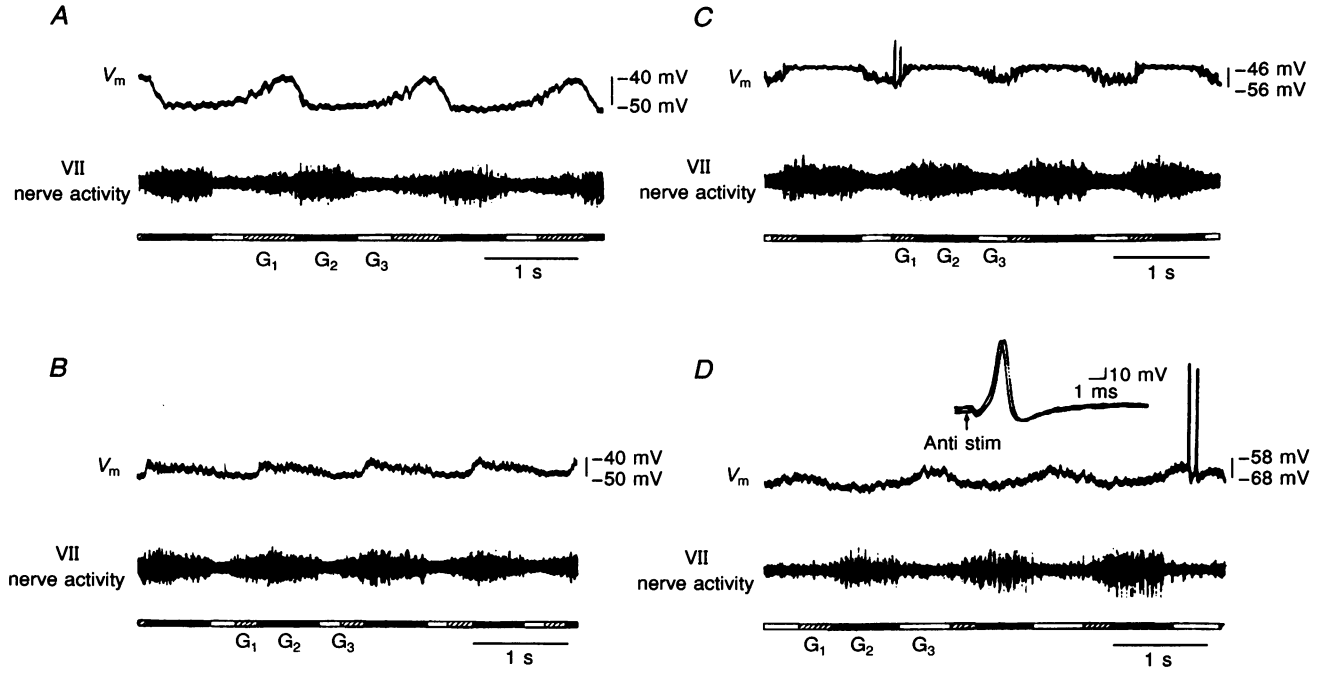

Figure 3. Examples of intracellular recordings from phase-bound VII motoneurons having different patterns of modulation with gill rhythmicity

Top traces: membrane potential (V_m); middle traces: whole VII nerve activity; bottom traces: marker bar showing successive phases of the gill cycle. *A*, G_1-type of motoneuron, showing a gradually increasing depolarization during the early phase of the gill burst, followed by a rapid decline. *B*, G_2-type motoneuron with a rapid onset of depolarization during the G_2 phase, followed by a gradual decline. *C*, G_{1-2}-type cell, showing a depolarization throughout the gill burst period. (The cell is actively hyperpolarized during the G_3 phase.) *D*, G_3-type cell, showing a depolarization during the interval between gill bursts. The inset shows, on an expanded time scale, four superimposed sweeps with antidromic action potentials of this cell (Anti stim, antidromic stimulation). The latency of the response varied with the cyclic changes in the membrane potential.

Membrane potential trajectories of respiratory neurons within the facial nucleus

Intracellular recordings were obtained from seventy-five respiratory-modulated neurons located within the VII nucleus region. Sixty of them were identified as VII motoneurons by antidromic activation. An example of antidromic action potentials in a motoneuron is shown in the inset in Fig. 3*D*. The latency for antidromic activation of these sixty neurons measured from the stimulus onset to the foot of antidromic spike was 0·4–0·8 ms (mean, 0·5 ± 0·1 ms; $n = 60$), with the conduction distance being about 1·0 mm. The remaining fifteen neurons could not be antidromically activated from the VII nerve.

Of the seventy-five cells, fifty-six had both gill- and lung-related respiratory modulation of their membrane potentials (44 motoneurons, 12 not antidromically activated (NAA) neurons). Membrane potential of the remaining nineteen cells was modulated only with the lung rhythmicity (16 motoneurons, 3 NAA neurons). We did not observe any cells showing modulation related to gill rhythmicity alone. The range of membrane potentials at the most negative level for neurons having both gill and lung activities was from −40 (our limit to accept the recording) to −75 mV (mean, −54 ± 10 mV). The range of the membrane potential for the cells showing only lung rhythmicity was −44 to −80 mV (mean, −62 ± 9·6 mV).

Patterns of membrane potential changes with gill rhythm. The patterns of respiratory modulation seen in individual neurons were highly repeatable from cycle to cycle and characteristic of individual cells. Based on the temporal relationship between the occurrence of the maximal depolarization of the membrane potential and the corresponding characteristic phases of the gill cycle in the whole VII nerve described above, we have classified the fifty-six gill-modulated neurons into three groups: group one ($n = 26$), depolarized in a clear temporal association with either G_1 or G_2, or both these phases; group two ($n = 24$), in which onsets and offsets of the period of depolarization could not be clearly ascribed to the transition points between distinct phases seen in the VII nerve activity (phase-spanning cells); and group three ($n = 6$), depolarized during the interval between gill bursts. Figure 3 shows examples of the membrane potential trajectories in typical neurons with phase-bound modulation, while Fig. 4 shows two cells of the phase-spanning type.

In eight of the twenty-six phase-bound neurons that were depolarized during the gill burst, the depolarization was confined to the G_1 phase (G_1 neurons; Fig. 3*A*). In another ten cells, the depolarization occurred only during the G_2 phase (G_2 neurons; Fig. 3*B*), while in the remaining eight cells, phasic depolarizations began at the onset of G_1 phase and terminated at the offset of the G_2 phase (Fig. 3*C*). For the latter group, some of the cells appeared to be phasically inhibited during G_3 rather than depolarized during phases G_{1-2} (see the last section of the Results). Finally, the six phase-bound neurons that were depolarized during the period between gill bursts were termed G_3 cells. Figure 3*D* shows the recording from such a cell.

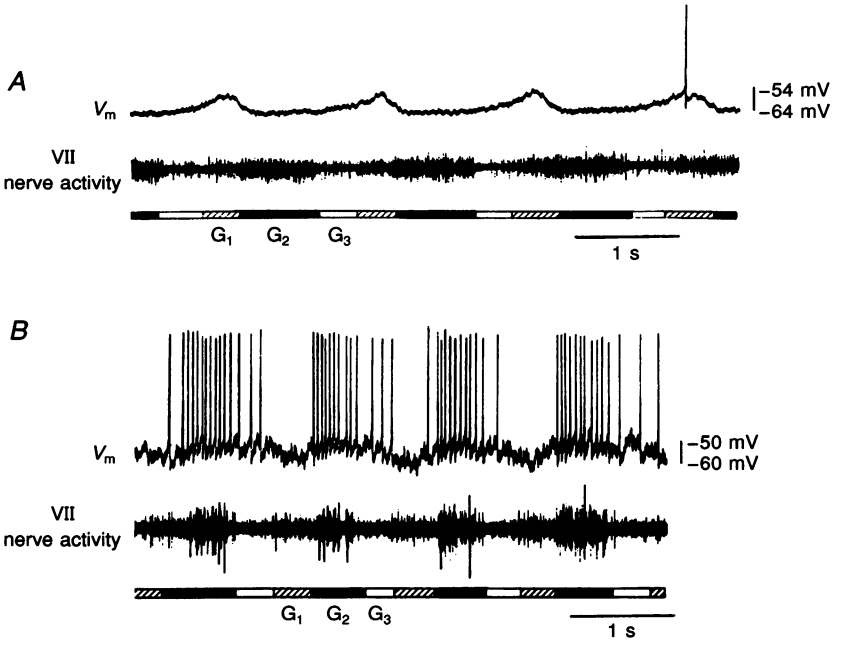

Figure 4. Examples of cells classified as phase spanning

A, $G_{3/1}$-type cell, with a depolarization that begins in the interval between the gill burst (G_3) and continues through the G_1 phase of the gill burst. *B*, $G_{2/3}$-type cell, with a depolarization that begins in the middle of phase G_1 and ending gradually during phase G_3. Traces as in Fig. 3.

Table 1. Resting membrane potentials and magnitudes of their gill-related modulations in different classes of gill-modulated cells

		Magnitude gill modulation (mV)		V_m (mV)	
Cell type	N*	Range	Mean ± S.D.	Range	Mean ± S.D.
G_1	8 (14%)	3–12	6 ± 3	40–70	54 ± 9
G_2	10 (18%)	3–10	6 ± 2	40–75	56 ± 13
G_{1-2}	8 (14%)	5–14	8 ± 4	40–75	48 ± 12
G_3	6 (11%)	5–15	9 ± 4	50–70	58 ± 8
$G_{2/3}$	20 (36%)	3–11	7 ± 2	40–70	54 ± 10
$G_{3/1}$	4 (7%)	4–13	9 ± 5	50–70	60 ± 8

V_m, resting membrane potential. * Number (N, as a percentage) of all gill-modulated cells.

Of the twenty-four phase-spanning neurons, in four, a maximal depolarization occurred between G_3 and G_1 ($G_{3/1}$ cells) (Fig. 4*A*), while in the remaining twenty, it was between G_2 and G_3 ($G_{2/3}$ cells) (Fig. 4*B*). Table 1 provides the information about the resting membrane potential and the magnitude of the gill-related modulation in all the gill-modulated cells. All these cells were also modulated in relation to the lung burst. This is described more fully below.

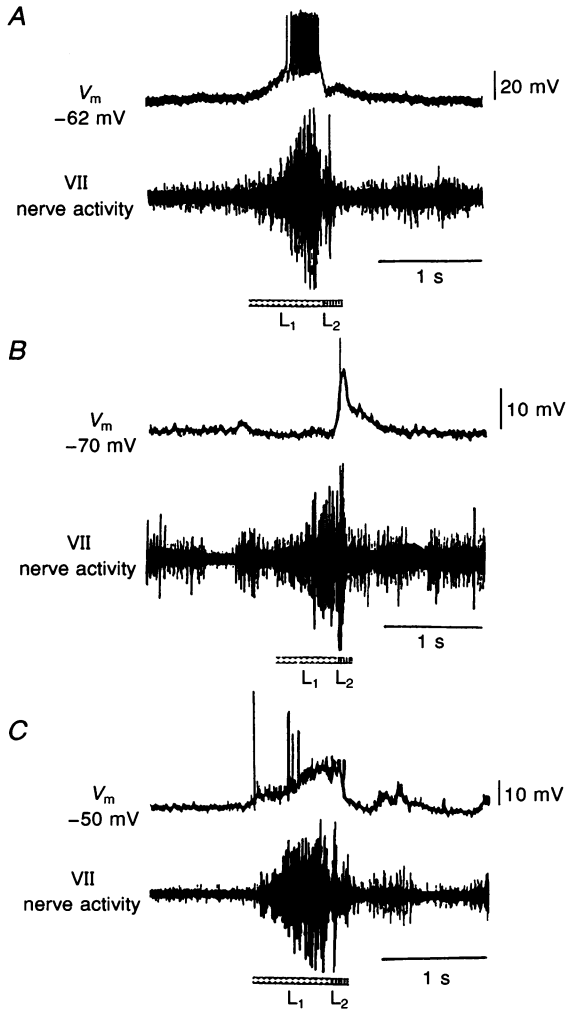

Figure 5. Facial motoneurons having three distinct patterns of membrane potential trajectories related to the fictive lung ventilation

A, L_1-type cell, showing a depolarization during the first phase of the lung burst. *B*, L_2-type cell, with a depolarization during the second phase of the lung burst. *C*, L_{1-2} cell, with a depolarization throughout the lung burst period. Top traces: membrane potential (V_m); middle traces: whole VII nerve activity; bottom traces: marker bar showing successive phases of the lung burst.

The overall shapes of membrane potential trajectories were different in different subpopulations of gill-modulated neurons. The G_1 cells had a 'ramp-like' depolarization followed by a rapid repolarization (Fig. 3*A*), whereas G_2 cells showed a rapid onset of depolarization followed by a gradual return of the membrane potential to the pre-burst level (Fig. 3*B*). In the remaining cell types (G_3, $G_{2/3}$ and $G_{3/1}$) the membrane potential showed gradual changes in both depolarizing and repolarizing directions (Figs 3*D* and 4).

Patterns of membrane potential changes with lung rhythm. Of the seventy-five neurons that changed their membrane potential in relation to the lung burst, seventy were depolarized at some phase of the burst. These seventy cells were classified into three groups: group one ($n = 38$), comprised of neurons that depolarized during the first phase of the lung burst (L_1); group two ($n = 17$), depolarized during the second phase of the lung burst (L_2); and group three ($n = 15$), depolarized throughout both phases of the lung burst (L_{1-2}). Figure 5 shows typical examples of these three cell types.

We did not find either phase-spanning cells, i.e. those with depolarizations starting and/or ending within one or the other phases of the lung cycle rather than at distinct transition points between adjacent phases or cells that depolarized during the period between lung bursts (L_3). However, in addition to the seventy cells described above, we identified five neurons with a distinct hyperpolarizing shift of the membrane potential during the L_1 phase of the lung burst and no distinct phase of depolarization. We

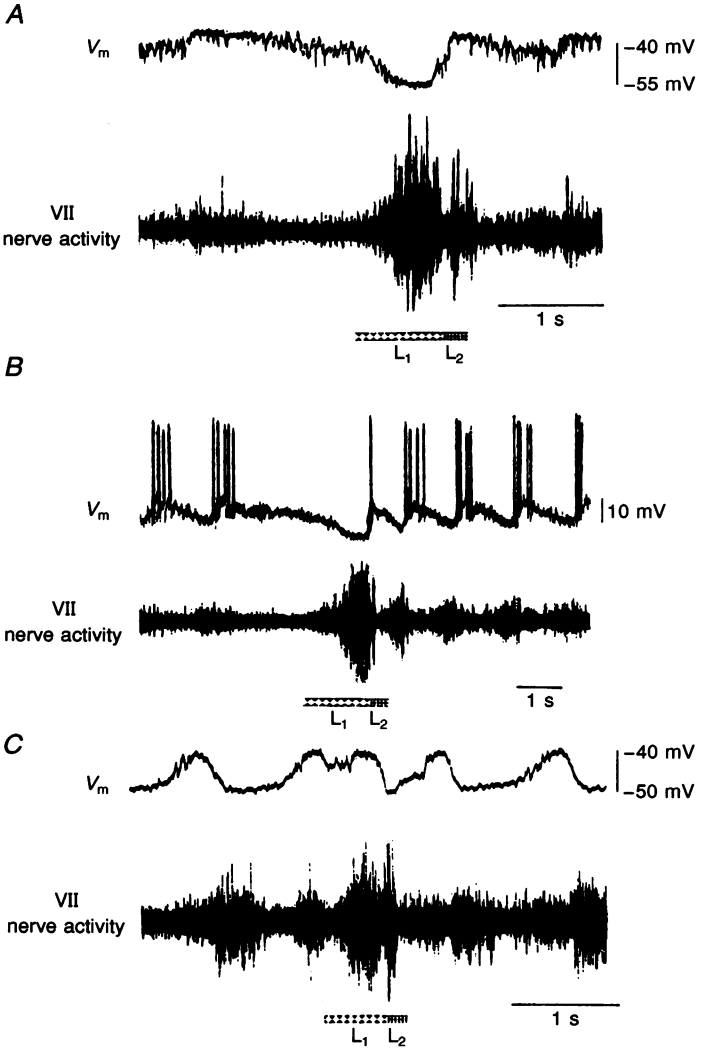

Figure 6. Examples of cells with distinct de- and/or hyperpolarizations during different phases of the lung burst

A, an L_{1h} cell showing only a hyperpolarization related to the L_1 phase of the lung burst. There was also a depolarization during the G_2 phase of the gill burst. *B*, a cell depolarized during the L_2 phase and hyperpolarized during L_1 phase (classified as L_2). There is also a pronounced gill-related modulation with $G_{3/1}$ pattern. *C*, cell depolarized during the L_1 and hyperpolarized during the L_2 phase (classified as L_1). There was also a gill-related modulation with the G_1 pattern. Traces as in Fig. 5.

Table 2. Resting membrane potentials and magnitudes of their lung-related modulations in different classes of lung-modulated cells

	Cells with gill modulation					Cells without gill modulation				
		Magnitude lung modulation (mV)		V_m (mV)			Magnitude lung modulation (mV)		V_m (mV)	
Cell type	N*	Range	Mean ± S.D.	Range	Mean ± S.D.	N*	Range	Mean ± S.D.	Range	Mean ± S.D.
L_1	33 (44%)	5–23	14 ± 4	40–70	54 ± 9	5 (7%)	7–23	15 ± 7	50–70	57 ± 8
L_2	12 (16%)	7–20	13 ± 4	40–70	60 ± 13	5 (7%)	7–16	11 ± 3	50–80	68 ± 13
L_{1-2}	8 (11%)	8–20	14 ± 5	40–60	50 ± 5	7 (9%)	9–23	14 ± 5	50–75	61 ± 7
L_{1h}	3 (4%)	9–27	16 ± 10	40–70	50 ± 17	2 (3%)	6–12	—	40–50	—

*N, number as a percentage of the total.

labelled them as L_{1h} because what appeared to primarily shape their membrane potential trajectory was a phasic inhibition bound to this phase. This was verified further in experiments described in the last section of the Results. Figure 6*A* shows an example of one such cell. Moreover, in the group of fifty-five neurons that depolarized during one specific phase of the lung burst (L_1 or L_2) there were twenty-nine in which there was also a distinct period of hyperpolarization in the other phase. Such hyperpolarizations occurred either in phase L_1 ($n = 16$ of the 17 cells that depolarized during L_2; Fig. 6*B*) or L_2 ($n = 13$ of the 38 cells that depolarized during L_1; Fig. 6*C*) of the lung burst. The cell in Fig. 6*B* shows a distinct hyperpolarization that is particularly profound during the late portion of phase L_1. Thus, this cell is similar to the one shown in Fig. 6*A* as far as the timing of its hyperpolarizing input, yet it is different because of the presence of a distinct depolarization during the subsequent phase (L_2). In contrast, Fig. 6*C* shows a cell that had a hyperpolarization during L_2 phase following a distinct depolarization during L_1 phase of the lung burst. Resting membrane potentials and magnitudes of the membrane potential modulation associated with the lung rhythm in different classes of cells are summarized in Table 2 for both neurons with and without gill modulation.

Relationship between magnitudes of lung and gill modulation of the membrane potential in cells showing both rhythmicities

Since both rhythmicities were present in the majority of cells, we assessed if magnitudes and/or patterns of modulation of the membrane potential with the two rhythms were related in individual neurons. For this quantitative approach we limited our analysis to cells in which we used the same type of electrode – potassium acetate. Thus, this analysis was done for forty-eight cells. As shown in Fig. 7, there is a relationship between the magnitudes of gill and lung modulations as measured by the maximal change in membrane potential associated with each rhythm. The linear regression for this relationship was statistically significant ($r = 0{\cdot}516$, $P < 0{\cdot}001$). No significant differences were found between motoneurons and NAA cells in the magnitude of their modulation of membrane potential with lung and gill rhythmicities, nor in the ratio of the magnitudes of the two phasic inputs. To elucidate further what might have been the source of this correlation, we evaluated the relationship between the resting membrane potential and the magnitude of respiratory modulations seen in individual cells. For the modulation with gill rhythmicity, there was a significant linear correlation in that larger magnitudes of respiratory modulation were

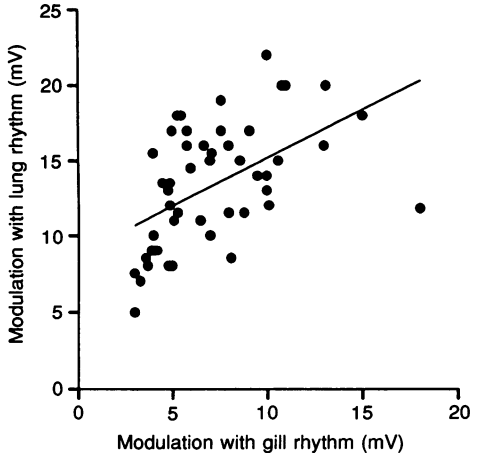

Figure 7. Relationship between the magnitudes of the gill and the lung modulations for 48 cells having both rhythmicities
The linear regression was significant ($r = 0{\cdot}516$, $P < 0{\cdot}001$).

associated with less hyperpolarized cells ($r = 0{\cdot}355$, $P < 0{\cdot}001$). For lung modulation, however, this relationship was not significant ($r = 0{\cdot}198$, $P > 0{\cdot}05$). The relationship for gill modulation might have reflected a relatively larger contribution of phasic inhibitory inputs to the respiratory modulation of membrane potentials in cells whose membrane potentials were further away from the equilibrium potential for Cl^- (see below).

The prevailing patterns of convergence of the lung- and gill-related modulations were those expected on the basis of the rates of occurrence of individual lung- and gill-related patterns (Tables 1 and 2). Thus, cells with the L_1 and $G_{2/3}$ combination represented 25% of the sample. The next most frequent were cells with L_1 and G_2 convergence (11%), followed by the L_2 and G_2 combination (9%). None of the patterns of convergence occurred with a probability significantly different from that expected on the basis of the rates of occurrence of individual lung- and gill-related patterns in the studied sample of fifty-six neurons.

Phasic inhibitory inputs to respiratory neurons

Although in our classification of respiratory cells we focused on the time course of occurrence of phasic depolarizations, for some neurons the modulation of their membrane potential might have been shaped to a large degree by phasic inhibitory inputs alone or in addition to excitatory ones. Examples suggesting that it may be the case have been presented in Fig. 6. To assess this possibility further, we have studied in more detail sixteen neurons (12 motoneurons, 4 NAA cells). These cells were selected because an initial inspection of their membrane potential trajectories suggested that they were actively hyperpolarized during a portion of either the gill or the lung cycle. In those neurons, we have evaluated the character of the synaptic noise using a fast time scale, high gain recordings (Fig. 8). We also assessed whether the hyperpolarizations seen in those cells could be reversed by either intracellular injections of a negative current or Cl^-, and determined whether the period of hyperpolarization was associated with a decrease in the somatic membrane resistance. Presumed inhibitory inputs were present in various phases of the lung burst or gill cycle in different neurons. In eight of those sixteen neurons, a presumed inhibitory input occurred during phase L_1 of the lung burst, in four neurons during phase L_2 of the lung burst, and in ten of those sixteen cells during G_1 or G_2 phases of the gill cycle (Figs 6, 8 and 9).

In nine out of those sixteen selected neurons, there was a clear IPSP-like synaptic noise during the period of hyperpolarization within the lung and/or gill cycle whereas in the remaining seven cells this phenomenon was not so obvious. The average membrane potential of the nine cells with IPSP-like synaptic noise was -44 ± 5 mV, while the remaining seven cells without the IPSP-like synaptic noise

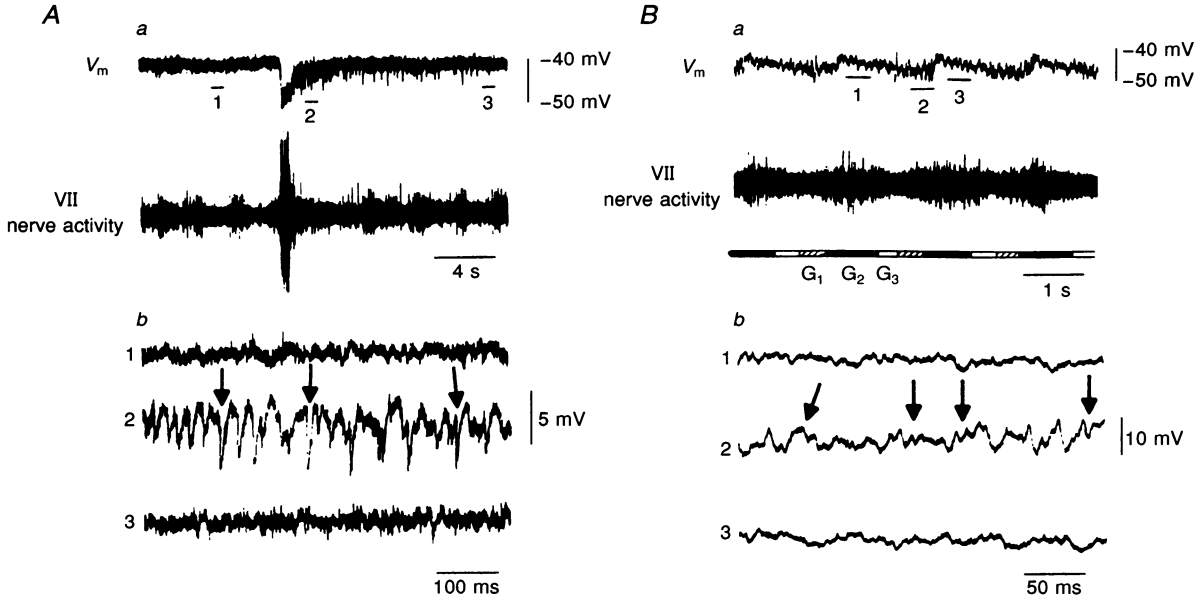

Figure 8. Examples of an IPSP-like noise occurring during different portions of the lung burst (*A*) or gill cycle (*B*)

A, a motoneuron with a large IPSP-like noise during and immediately following the lung burst. *B*, G_2-type cell that was hyperpolarized during the G_1 and G_3 phases. Lower panels (*b*) in both *A* and *B* show three samples of high gain recordings from different portions of the membrane potential (V_m) record shown in the corresponding upper panels (*a*) and numbered 1, 2 and 3, as in the lower panels. Arrows show selected large IPSP-like wavelets. Note that such wavelets, characterized by a rapid hyperpolarization and a gradual repolarization, are almost absent from traces 1 and 3.

had an average membrane potential of -63 ± 8 mV. This difference suggests that the IPSP-like noise was not observed in the latter cells because their membrane potential was relatively close to the equilibrium potential for Cl^-, but specific tests with passing of a depolarizing current were not performed to verify this possibility. Figure 8*A* shows an example of a cell with a large amplitude IPSP-like synaptic noise that occurred during, and immediately following, the lung burst, while Fig. 8*B* shows an example of such noise occurring during the G_1 phase of the gill cycle in another cell.

In all eight cells in which it was done, the hyperpolarizing phase occurring with either gill ($n = 6$) or lung ($n = 8$) rhythmicity was abolished or reversed so that it was converted to an additional depolarizing wave during a negative current injection (0·5–2·0 nA). Figure 9 shows examples of such reversals. In Fig. 9*A a*, a G_2 NAA cell had a hyperpolarization with IPSP-like synaptic noise during the G_3 and G_1 phases of the gill cycle. This inhibition was reversed during 1 nA negative current injection (Fig. 9*A b*). In Fig. 9*B a*, a motoneuron showed a hyperpolarization during the late part of the L_1 phase that was reversed during a 0·5 nA hyperpolarizing current injection (Fig. 9*B b*).

In another eight cells showing a period of presumed postsynaptic inhibition, we performed intracellular injection of Cl^- from a KCl-filled pipette. The phasic hyperpolarization of the membrane potential was reduced or reversed to a depolarizing wave within 1–5 min of such injections (1–10 nA). This was observed during phasic inhibitions related to either gill ($n = 4$) or lung bursts ($n = 8$). An example of reversal of both lung and gill rhythm-related phasic inhibitions following Cl^- injection is shown in Fig. 10.

As the Cl^--mediated inhibition is associated with a decrease in the somatic membrane resistance (R_n), in five motoneurons and one NAA cell we measured the difference in R_n between the periods of maximal depolarization and hyperpolarization occurring with gill rhythmicity. The mean maximal negative membrane potential for this group was -50 ± 11 mV and the average magnitude of its respiratory modulation was $10·8 \pm 2·1$ mV. In individual neurons, R_n decreased by 0·7–8·1 MΩ (mean, $5·2 \pm 2·6$ MΩ) during the period of hyperpolarization with the decrease being highly significant in all cells at $P < 0·0005$. Two of these six neurons were also submitted to tests with injection of a hyperpolarizing current and a reversal of the presumed inhibitory input was obtained in both cases.

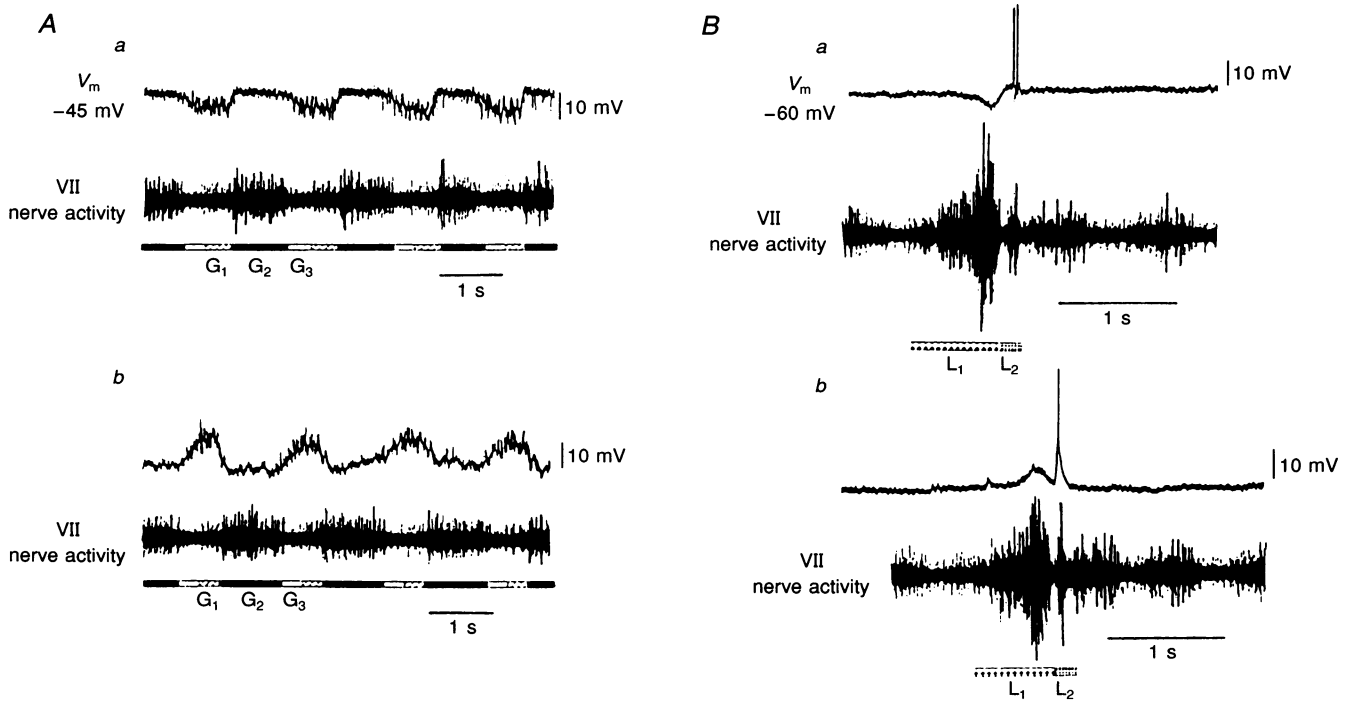

Figure 9. Examples of hyperpolarization-induced reversals of phasic inhibitory inputs during distinct phases of respiratory cycles in two neurons

A, neuron showing a hyperpolarization during the G_1 and G_3 phases of the gill cycle. *a*, control record; *b*, during continuous application of a hyperpolarizing current (1 nA). *B*, motoneuron with lung modulation only that was hyperpolarized during the L_1 phase of the lung burst. *a*, control record; *b*, during a continuous application of a hyperpolarizing current (0·5 nA).

DISCUSSION

In the present experiments, we found that membrane potentials of the majority (75%) of the respiratory-modulated neurons in the region of the VII nucleus are modulated with both gill and lung rhythms, while the remaining 25% show a modulation with lung rhythm only. This distribution was similar for both identified motoneurons and cells that were not antidromically activated following stimulation of the VII nerve. We found no cells that had their membrane potential modulated with the gill rhythm alone. In a portion of the cells, the presence of a phasic inhibition mediated by Cl^- was detected, showing that both excitatory and inhibitory phasic respiratory inputs determine the shape of their membrane potential trajectories.

The particular distribution of lung and gill rhythmicities in the population of neurons that we studied can be related to the respiratory activity of muscles innervated by the VII nerve in tadpoles and bullfrogs. Studies of activities in respiratory muscles or nerves in amphibians (deJongh & Gans, 1969; Nieuwenhuys & Opdam, 1976; Sakakibara, 1984; Kogo, Perry & Remmers, 1994) show that some muscles (e.g. subhyoid) participate only in lung ventilation whereas others show rhythmic contractions with both buccal and lung rhythms (e.g. posterior intermandibular). To our knowledge, no muscles innervated by the VII nerve show buccal rhythmicity alone. Thus, the patterns of rhythmicities in the neurons in the VII nucleus region that we studied are in keeping with the patterns of activities seen in the muscles innervated by the VII nerve. What is noteworthy, however, is that the distribution and convergence pattern of the two rhythmicities in motoneurons was similar to that in non-antidromically activated (NAA) cells. Although some of the latter could be motoneurons that we failed, for technical reasons, to excite antidromically, it is likely that this group includes interneurons located in the region of the VII nucleus. If this is the case, the presence of both rhythms in most of the NAA cells shows that the two rhythmic inputs, coming from brainstem sites that are presumably distinct, may be integrated at a pre-motor level rather than, or in addition to, converging within motoneurons.

The mechanical aspect of breathing in amphibians is quite complex because of the presence of two complimentary gas exchange mechanisms, i.e. gills and lungs (deJongh & Gans, 1969; West & Jones, 1975). Although these two rhythmic

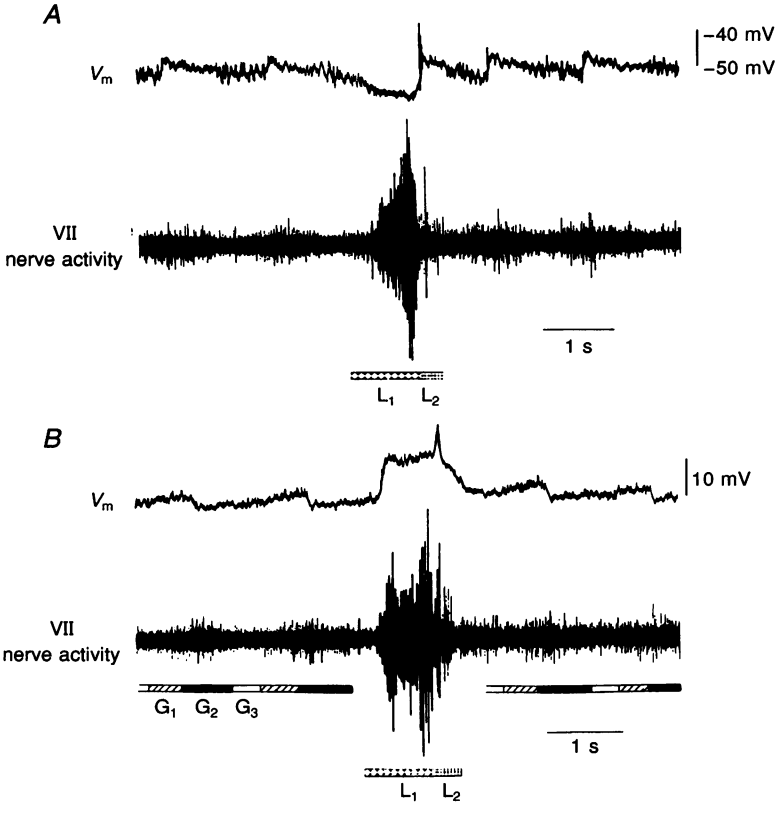

Figure 10. Example of a reversal of phasic inhibitory inputs following injection of Cl^-

In control conditions (*A*), the cell was hyperpolarized during L_1 and G_1 phases of the lung and gill bursts, respectively. In *B*, following injection of Cl^- (−2 nA, 4 min), a depolarization is seen instead during the L_1 and G_1 phases.

behaviours use many of the same muscles of the buccopharyngeal cavity, their corresponding central pattern generators are likely to be distinct as has been proposed for another species with these modes of gas exchange, i.e. the lungfish (Fishman, Galante & Pack, 1989). In frogs, the two rhythms can be selectively abolished by appropriate brainstem lesions (McLean, Perry, Kogo & Remmers, 1991).

Previous attempts to understand the sequence of ventilatory events in frogs have used recordings of pressures from the respiratory organs and/or activity from various cranial muscles and nerves (deJongh & Gans, 1969; West & Jones, 1975; Sakakibara, 1984; Kogo *et al.* 1994). According to these studies, gill ventilation is relatively simple and consists of an almost continuous raising and lowering of the buccal floor at a frequency of fifty to a hundred per minute. However, our studies of respiratory neurons reveal that the gill cycle has three distinct phases. Three phases have also been described for the gill ventilatory cycle in other species: in the carp, three phases were identified by observation of mechanical events (Ballintijn, 1984; Ballintijn & Punt, 1985); and, in the lamprey, they were revealed by recording from respiratory motoneurons (Rovainen, 1977; Thompson, 1985). In the lamprey, the gill cycle consists of an initial phase with a low amplitude EPSP, followed by a larger EPSP burst, and finally by an IPSP phase. Thus, our observations identify similar patterns in the VII nucleus of amphibia to those found in these other species. However, in contrast to our results, all motoneurons studied in lamprey showed the three-phase input (Thompson, 1985).

Based on studies in frogs (deJongh & Gans, 1969; West & Jones, 1975; Sakakibara, 1984; Kogo *et al.* 1994), lung ventilation involves the following complex sequence of events: aspiration of air into the buccal cavity (buccal inhalation or pre-L-phase); opening of the glottis allowing the lung to empty (expiration phase); closing of the nostrils combined with a contraction of buccal musculature to inflate the lung (lung inflation phase) followed by closing of the glottis (post-L-phase). Within this sequence, up to six phases of the pulmonary ventilatory cycle have been distinguished by Sakakibara (1984) based on the recording of lung pressure changes. He also recorded activity of the VII nerve during the pulmonary ventilatory cycle in adult bullfrogs, *Rana catesbeiana*, and reported a small amount of activity during the initial buccal inhalation phase followed by two distinct peaks: the first coincided with the phase of lung emptying (expiration); the second with the phase of inspiration when the lung is filled by action of the buccal force pump. However, because the timing is not clear in the experimental record shown in that study, it is difficult to relate the phases we identified to the two peaks in the facial nerve reported by Sakakibara (1984).

In another study, Kogo *et al.* (1994) did not record facial nerve activity. Instead, they recorded from branches of the trigeminal, vagal and hypoglossal nerves and divided the act of pulmonary ventilation into four phases, one of which was the expiratory phase (E) that preceded the period of pulmonary filling (inspiration, I). Based on observation of the whole VII nerve activity and classification of membrane potential trajectories in individual neurons, we identified only three distinct phases of the lung cycle. This smaller number of phases distinguished in our study by recording from the VII nerve and its individual motoneurons, may result from us recording from only one cranial nerve. However, comparison of our records with those of Kogo *et al.* (1994) suggests that our phase L_1 may correspond to the combined phases pre-L and E, while our L_2 phase corresponds to their I phase. The two peaks of activity in the latter study are about even in duration, whereas our phase L_2 is about five times shorter than L_1. Kogo *et al.* (1994) also found two peaks in the activity of the vagus nerve. They occurred in their I phase and what they called the post-L phase. These peaks showed a similar temporal relationship to our L_1 and L_2 phases.

Thus, the observations in the present study do not allow us to reconcile fully our L_1 and L_2 phases with those described by previous investigators. This is not surprising since previous studies have been conducted in adult animals, while our studies are in a fully deafferented brain *in vitro*, harvested from larval specimens at intermediate stages of development. Additional studies are needed with recordings from multiple cranial nerves and of lung pressure to determine whether the two peaks, L_1 and L_2, represent peaks in the pre-L/E and I phases or, alternatively, in the I and post-L phases. In either case, the presence in our sample of neurons depolarized during both L_1 and L_2 phases suggests that a simple analogy with inspiratory and expiratory neurons of mammals may not be appropriate because it leads to classification of some neurons as being both inspiratory and expiratory. Likewise, Kogo & Remmers (1994) could not identify in adult amphibia any cells that fired only in the period that they functionally regarded as expiration.

Although the classification of neurons in this study was primarily based on the timing of phasic excitatory inputs, we also obtained evidence for phasic postsynaptic inhibition. The presence of Cl^--mediated inhibition was revealed in eight neurons by the intracellular injection of Cl^-. Consistent with this finding, reversal of a phasic hyperpolarization occurred in eight other neurons during a current-induced hyperpolarization; also, in all six cells studied, somatic membrane resistance decreased during the period of hyperpolarization. Phasic inhibitions were present during various portions of either gill or lung respiratory cycles and in both motoneurons and NAA cells. Thus, the Cl^--mediated inhibition probably makes an important contribution to the shaping of respiratory motor outputs for both the gill and lung ventilation. Since the inhibitory effects could often be reversed after short periods of Cl^- injection, at least some of those inhibitory

synapses seem to be located near the soma of the neurons studied. Similarly, phasic inhibitory inputs contribute to the shaping of the respiratory activity in lampreys (Thompson, 1985; Russell, 1986) and are consistently present in most mammalian respiratory neurons, including motoneurons (e.g. Ballantyne & Richter, 1984).

In conclusion, in the present study, we have used recordings from the whole VII nerve and individual VII motoneurons to elucidate the sequence of central neural respiratory events at intermediate stages of tadpole development. Further studies of respiratory neurons in amphibia at different developmental stages are needed to determine which features of the respiratory network in tadpoles are preserved in adult species.

Ballantyne, D. & Richter, D. W. (1984). Post-synaptic inhibition of bulbar inspiratory neurons in the cat. *Journal of Physiology* **348**, 67–87.

Ballintijn, C. M. (1984). The respiratory function of gill filament muscles in the carp. *Respiration Physiology* **60**, 59–74.

Ballintijn, C. M. & Punt, G. J. (1985). Gill arch movements and the function of the dorsal gill arch muscles in the carp. *Respiration Physiology* **60**, 39–57.

Berger, A. J. (1990). Recent advances in respiratory neurobiology using *in vitro* methods. *American Journal of Physiology* **259**, L24–29.

Burggren, W. W. (1984). Transition of respiratory processes during amphibian metamorphosis: From egg to adult. In *Respiration and Metabolism of Embryonic Vertebrates*, ed. Seymour, R. S., pp. 31–53. Junk, Dordrecht, Netherlands.

Burggren, W. W. & Just, J. J. (1992). Developmental changes in physiological systems. In *Environmental Physiology of the Amphibians*, ed. Feder, M. E. & Burggren, W. W., pp. 467–530. University of Chicago Press, Chicago and London.

Burggren, W. W. & West, N. H. (1982). Changing respiratory importance of gills, lungs and skin during metamorphosis in the bullfrog, *Rana catesbeiana*. *Respiration Physiology* **47**, 151–164.

Cohen, A. H., Dobrov, T. A., Li, G., Kiemel, T. & Baker, M. T. (1990). The development of the lamprey pattern generator for locomotion. *Journal of Neurobiology* **21**, 958–969.

deJongh, H. J. & Gans, C. (1969). On the mechanism of respiration in the bullfrog, *Rana catesbeiana*: A reassessment. *Journal of Morphology* **127**, 259–290.

Ezure, K. (1990). Synaptic connections between medullary respiratory neurons and considerations on the genesis of respiratory rhythm. *Progress in Neurobiology* **35**, 429–450.

Feldman, J. L. & Smith, J. C. (1989). Cellular mechanisms underlying modulation of breathing pattern in mammals. *Annals of the New York Academy of Sciences* **563**, 114–130.

Feldman, J. L., Smith, J. C., Ellenberger, H. H., Connelly, C. A., Liu, G. S., Greer, J. J., Lindsay, A. D. & Otto, M. R. (1990). Neurogenesis of respiratory rhythm and pattern: emerging concepts. *American Journal of Physiology* **259**, R879–886.

Fishman, A. P., Galante, R. J. & Pack, A. I. (1989). Diving physiology. Lungfish. In *Comparative Pulmonary Physiology*, ed. Wood, S. C., pp. 645–676. Dekker, New York.

Galante, R., Smith, E., Kubin, L. & Pack, A. I. (1992). Developmental changes in respiratory neural output in larval form of *Rana catesbeiana*. *Society for Neuroscience Abstracts* **18**, 125.

Kogo, N., Perry, S. F. & Remmers, J. E. (1994). Neural organization of the ventilatory activity in the frog, *Rana catesbeiana*. I. *Journal of Neurobiology* **25**, 1067–1079.

Kogo, N. & Remmers, J. E. (1994). Neural organization of the ventilatory activity in the frog, *Rana catesbeiana*. II. *Journal of Neurobiology* **25**, 1080–1094.

Liao, G. S., Kubin, L., Galante, R., Pack, A. I. & Fishman, A. P. (1993). Membrane potential trajectories of respiratory neurons in the VIIth nucleus studied *in vitro* at intermediate stages of development in tadpoles (*Rana catesbeiana*). *Society for Neuroscience Abstracts* **19**, 558.

McLean, H. A., Perry, S. F., Kogo, N. & Remmers, J. E. (1991). An important area for respiratory rhythmogenesis in the medulla of the frog *Rana catesbeiana*: an *in vitro* study using the hemisected brainstem. *Society for Neuroscience Abstracts* **17**, 198.

Nieuwenhuys, R. & Opdam, P. (1976). Structure of the brainstem. In *Frog Neurobiology*, ed. Llinas, R. & Precht, W., pp. 811–855. Springer, New York.

Pack, A. I., Galante, R. J., Walker, R. E., Kubin, L. & Fishman, A. P. (1993). Comparative approach to neural control of respiration. In *Respiratory Control Central and Peripheral Mechanisms*, ed. Speck, D. F., Dekin, M. S., Revelette, W. R. & Frazier, D. T., pp. 52–57. The University Press of Kentucky, Lexington, KY, USA.

Rovainen, C. M. (1977). Neural control of ventilation in the lamprey. *Federation Proceedings* **36**, 2386–2389.

Russell, D. F. (1986). Respiratory pattern generation in adult lampreys (*Lampetra fluviatilis*): interneurons and burst resetting. *Journal of Comparative Physiology* A **158**, 91–102.

Russell, D. F. & Wallén, P. (1983). On the control of myotomal motoneurons during fictive swimming in the lamprey spinal cord *in vitro*. *Acta Physiologica Scandinavica* **117**, 161–170.

Sakakibara, Y. (1984). The pattern of respiratory nerve activity in the bullfrog. *Japanese Journal of Physiology* **34**, 269–282.

Shelton, G., Jones, D. R. & Milsom, W. K. (1986). Control of breathing in ectothermic vertebrates. In *Handbook of Physiology*, section 3, *The Respiratory System*, vol. 2, ed. Cherniack, N. S. & Widdicome, J. K., pp. 857–909. American Physiological Society, Bethesda, MD, USA.

Sillar, K. T., Simmers, A. J. & Wedderburn, J. F. S. (1992). The post-embryonic development of cell properties and synaptic drive underlying locomotor rhythm generation in *Xenopus* larvae. *Proceedings of the Royal Society* B **249**, 65–70.

Sillar, K. T., Wedderburn, J. F. S. & Simmers, A. J. (1991). The development of swimming rhythmicity in post-embryonic *Xenopus laevis*. *Proceedings of the Royal Society* B **246**, 147–153.

Smith, J. C. & Feldman, J. L. (1987). *In vitro* brainstem–spinal cord preparations for study of motor systems for mammalian respiration and locomotion. *Journal of Neuroscience Methods* **21**, 321–333.

Suzue, T. (1984). Respiratory rhythm generation in the *in vitro* brainstem–spinal cord preparation of the neonatal rat. *Journal of Physiology* **354**, 173–183.

Taylor, A. C. & Kollros, J. (1946). Stages in the normal development of *Rana pipiens* larvae. *Anatomical Reviews* **94**, 7–23.

Thompson, K. J. (1985). Organization of inputs to motoneurons during fictive respiration in the isolated lamprey brain. *Journal of Comparative Physiology* **157**, 291–302.

WEST, N. H. & BURGGREN, W. W. (1982). Gill and lung ventilatory responses to steady-state aquatic hypoxia and hyperoxia in the bullfrog tadpole. *Respiration Physiology* **47**, 165–176.

WEST, N. H. & BURGGREN, W. W. (1983). Reflex interactions between aerial and aquatic gas exchange organs in the larval bullfrog. *American Journal of Physiology* **244**, R770–777.

WEST, N. H. & JONES, D. R. (1975). Breathing movements in the frog *Rana pipiens*. I. The mechanical events associated with lung and buccal ventilation. *Canadian Journal of Zoology* **53**, 332–344.

Acknowledgements

We are grateful to Mr Daniel C. Barrett for excellent secretarial support. The studies were supported in part by NIH grants HL-49486 and HL-07713.

Author's email address

A. I. Pack: pack@mail.med.upenn.edu

Received 2 May 1995; *accepted 15 November 1995.*